The HF Surface Wave Radar WERA. Part II: Spectral Analysis of Recorded Data

Salvatore Maresca, Maria Greco, Fulvio Gini
Dept. of Information Engineering, University of Pisa, via G. Caruso 16, 56122 Pisa (PI), Italy
{salvatore.maresca, m.greco, f.gini}@iet.unipi.it

Raffaele Grasso, Stefano Coraluppi
NATO Undersea Research Centre, viale S. Bartolomeo 400, 19126 La Spezia (SP), Italy
{grasso, coraluppi}@nurc.nato.int

Nicolas Thomas
SAS ActiMar, 36 Quai de la Douane, 29200 Brest, France
nicolas.thomas@actimar.fr

***Abstract*—This paper covers the second part of the analysis of data recorded by the surface wave (SW) over-the-horizon (OTH) WEllen RAdar (WERA). Data were collected by two WERA systems, on May 13th 2008, during the NURC experiment in the Bay of Brest, France. The principal aim of this work is to provide an accurate characterization of the spectral components of the received signal. Secondly, this information is exploited in order to provide a simple and reliable spectral modeling tool. For this reason, auto-regressive (AR) models, also known as linear prediction (LP) models have been investigated. Our results show that at long distances, when the clutter-to-noise power ratio (CNR) is small, the main components of the spectrum can be reasonably described by an AR(12) model, with a good compromise between accuracy and simplicity. As the CNR increases higher–orders are instead to be preferred.**

I. INTRODUCTION

High-frequency surface-wave radar (HFSWR) systems are particularly attractive for remote sea-state sensing by virtue of their over-the-horizon scanning capability [1]. Low-power HFSWRs can be found operating from the coast or on board of ships. This is the case of the WEllen RAdar (WERA), developed at the University of Hamburg and mainly devoted to remote sensing purposes [2], [3]. By exploiting the good conductivity of sea water in the lower HF band (3–15 MHz), HFSWRs are successfully used for detecting vessels and ships at long distances in the context of maritime surveillance and borders monitoring. In fact, they are able to solve the problem of line-of-sight (LOS) coverage typical of microwave radars and do not suffer from the periodic coverage of satellite based sensors [4], [5]. However high-power systems are quite complex and expensive, so even growing interest is focused on low-power HFSWRs, as WERA.

The contribution of HFSW sea clutter is produced by specific spectral components of the surface-height wavefield. First-order Bragg scattering is due to those ocean waves of half of the radar wavelength which travel towards and away from the radar site. The Doppler spectrum of the backscattered signal then contains two lines, corresponding to the phase velocities of the scattered ocean waves. These frequencies often deviate from the theoretically known values in non-moving waters. This phenomenon is due to an underlying surface current [6], [7]. Furthermore, in addition to the Bragg scattering returns, a more complicated feature is referred to as second-order scattering.

The working range of a HFSW radar depends not only on the attenuation of the electromagnetic wave during the transmitter-target-receiver path, but also on the scattering strength of the target, atmospheric noise and noise due to radio interference [1]. In fact, the ionosphere is prone to propagate interference at long distances, especially at night. Furthermore, external interference from natural and man-made sources typically masks the entire range-Doppler search space and is characterized by a spatial covariance matrix that is time-varying or non-stationary over the coherent processing interval (CPI). This physical phenomenon may arise from a number of causes. For instance, the dynamic properties of the ionosphere layers propagating the HF interference, the variation in geometry between radar receiver and interference sources and the impulsive nature of the sources [1], [8]. For all these reasons, OTH systems still represent a great challenge for the scientific community [2].

Regarding ship detection, the task is to resolve targets in the temporal or in the Doppler frequency domain from the same background clutter exploited for sea-state sensing. The two problems are thus in many ways complementary. In fact, the presence of clutter is unwelcome as far as ship detection is concerned, while the presence of ship returns can negatively affect the extraction of oceanographic parameters. For all these reasons, in the past years there has been much interest in trying to develop new spectral techniques for modeling the return from the sea, with the ultimate goals of enhancing performances in both target detection via clutter-suppression

978-1-4244-5813-4/10/$26.00 ©2010 IEEE

Report Documentation Page

Form Approved
OMB No. 0704-0188

1. REPORT DATE	2. REPORT TYPE	3. DATES COVERED
MAY 2010		**00-00-2010 to 00-00-2010**

4. TITLE AND SUBTITLE	5a. CONTRACT NUMBER
The HF Surface Wave Radar WERA. Part II: Spectral Analysis of Recorded Data	5b. GRANT NUMBER
	5c. PROGRAM ELEMENT NUMBER
6. AUTHOR(S)	5d. PROJECT NUMBER
	5e. TASK NUMBER
	5f. WORK UNIT NUMBER
7. PERFORMING ORGANIZATION NAME(S) AND ADDRESS(ES) **University of Pisa,Dept. of Information Engineering,via G. Caruso 16,56122 Pisa (PI), Italy,**	8. PERFORMING ORGANIZATION REPORT NUMBER
9. SPONSORING/MONITORING AGENCY NAME(S) AND ADDRESS(ES)	10. SPONSOR/MONITOR'S ACRONYM(S)
	11. SPONSOR/MONITOR'S REPORT NUMBER(S)

12. DISTRIBUTION/AVAILABILITY STATEMENT
Approved for public release; distribution unlimited

13. SUPPLEMENTARY NOTES
See also ADM002322. Presented at the 2010 IEEE International Radar Conference (9th) Held in Arlington, Virginia on 10-14 May 2010. Sponsored in part by the Navy.

14. ABSTRACT
This paper covers the second part of the analysis of data recorded by the surface wave (SW) over-the-horizon (OTH) WEllen RAdar (WERA). Data were collected by two WERA systems, on May 13th 2008, during the NURC experiment in the Bay of Brest, France. The principal aim of this work is to provide an accurate characterization of the spectral components of the received signal. Secondly, this information is exploited in order to provide a simple and reliable spectral modeling tool. For this reason, auto-regressive (AR) models, also known as linear prediction (LP) models have been investigated. Our results show that at long distances, when the clutter-tonoise power ratio (CNR) is small, the main components of the spectrum can be reasonably described by an AR(12) model, with a good compromise between accuracy and simplicity. As the CNR increases higher?orders are instead to be preferred.

15. SUBJECT TERMS

16. SECURITY CLASSIFICATION OF:			17. LIMITATION OF ABSTRACT	18. NUMBER OF PAGES	19a. NAME OF RESPONSIBLE PERSON
a. REPORT **unclassified**	b. ABSTRACT **unclassified**	c. THIS PAGE **unclassified**	**Same as Report (SAR)**	**6**	

techniques [9] and sea current sensing [10], by means of knowledge-based receiver configurations.

This paper deals with the spectral analysis of sea clutter using signals received by two concurrently operating WERA systems and it is organized as follows. A brief overview about WERA and the NURC experiment in the Bay of Brest (France) is provided in section II. In Section III a qualitative study about the main spectral components of the HF signal is carried out, while in Section IV the AR modeling of sea clutter spectrum is presented. Conclusions are instead drawn in Section V, in addition with some guidelines about future work.

II. WERA System and Experiment Description

The WERA system is essentially a shore based remote sensing system for monitoring ocean surface currents, wave spectra and wind direction. Its development has been carried out in 1995 at the University of Hamburg by K. W. Gurgel [2], [3]. Data were collected during the NURC experiment at Brest (Brittany, France), on the 13th of May 2008 [11]. The two WERA systems, respectively located at Brezellec (Latitude 48° 4' 8'', Longitude 4° 40' 0'') and Garchine (Latitude 48° 30' 10'', Longitude 4° 46' 32'') are owned by the French Service Hydrographique et Océanographique de la Marine (SHOM) and operated by the company SAS ActiMar. They were located parallel to the coast and aligned towards the true North with angles of 20° and 339°, respectively. Data records occurred every twenty minutes at each receiver site (i.e. Brezellec and Garchine) and last for 8 minutes and 52 seconds (corresponding to a CPI of 532 seconds), for a total of 2048 measurements with a chirp duration of 0.26 s, suitable for sea surface variability. Both the WERA systems worked at frequencies comprised between 12.190 and 12.565 MHz [12]. Bandwidth was set to 100 kHz (i.e. the range resolution is 1.5 km). For each chirp, 100 range samples were collected (for a maximum range of 150 km) [13].

III. Spectral Analysis

This paper is devoted to analyze and model the spectral features of the received HF signal. Since the receiver is a 16 element linear array of quarter-wavelength monopoles, initially a qualitative analysis was carried out for each antenna separately [14]. Before the statistical analysis, data have been beamformed by means of a simple rectangular window [15]. Two different data records have been considered, as representative of all the files: Brezellec dataset no. 8 (since 02:30:00 through 02:38:52 UTC) and Garchine dataset no. 6 (since 01:40:00 through 01:48:52 UTC). The aim is to focus our attention on the most important features of HF signals.

A. Sea clutter analysis

A two-dimensional color plot describes the behavior of the estimated power spectral density (PSD) in [dB] as a function of the range cells (rows) and of the Doppler frequency (columns), as shown in Fig. 1 for the 8th file recorded at Brezellec. A 512 samples window (corresponding to 133.12 s) and an azimuth angle of 15° have been considered. For the majority of range cells, two lines, which are related to the advancing (positive frequency) and receding (negative frequency) waves are easily recognized. The frequency separation Δf between the two first order Bragg peaks can be evaluated using the following formula [1]:

$$\Delta f = 2\sqrt{\frac{g \cdot f_c}{\pi \cdot c}}, \qquad (1)$$

where g is the acceleration due to gravity, c is the speed of light and f_c is the centre–band frequency. The Doppler separation corresponds to about 0.72 Hz for all the operative frequencies comprised between 12.190 and 12.565 MHz. Second-order peaks are well-defined in the first forty range cells. In this interval sea clutter level dominates both targets, and noise. Anyway, as we move away from the receiving radar, the CNR decreases and the two Bragg peaks are less defined, with the final result that background noise overcomes them. In this region sea clutter tends to become a white random process.

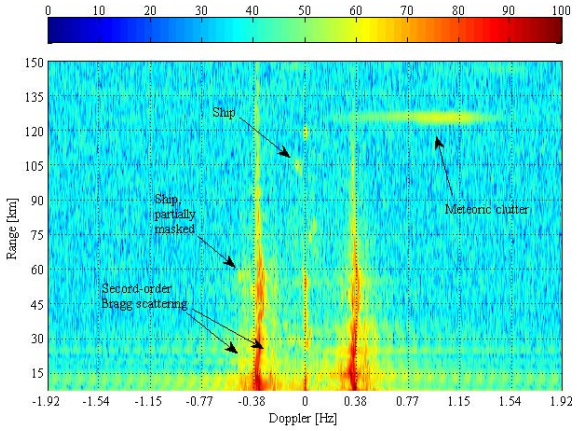

Figure 1. Brezellec dataset no. 8: clutter PSD in [dB] for an azimuth angle of 15°.

Together with sea clutter, especially for high CNR levels, the contribution of land-scattered echoes around the dc frequencies can be significant. In addition, the two Bragg peaks are subject to a frequency modulation. Rapid changes (e.g. turbulences) in the sea waves movement around rock cliffs lead to an evident broadening of the two Bragg frequencies [14], as shown in Fig. 2 for the 6th file recorded at Garchine. This phenomenon happens for all the files collected at Garchine, thanks to the presence of large islands (e.g. Ile d'Ouessant) at relatively small distance from WERA.

B. Interferences analysis

In HFSWRs, sea clutter is not the only type of signal we can observe, since systems are prone to a number of interference sources, both natural and man-made. The former usually consist of large returns (horizontal lines) that cover a large portion of the Doppler space. In this specific case they extend from about 0.20 to 1.60 Hz and manifest approximately around range cell 85 (about 126 km away from the coast), as shown in Fig. 1. These interferences are

responsible of the heavy-tailed behaviour of clutter amplitude described in [11]. They are principally due to unwanted propagation modes through the ionosphere and/or meteor trails echoes.

The second type of interference is represented by radio frequency interference (RFI), as shown in Fig. 2. These returns mask both sea clutter and ship echoes in even larger portions of the range-Doppler (RD) space. In fact they appear in certain Doppler frequencies intervals as vertical lines extending for all the defined range. For overcoming this serious problem an algorithm was proposed in [12] for estimating and then removing RFI noise.

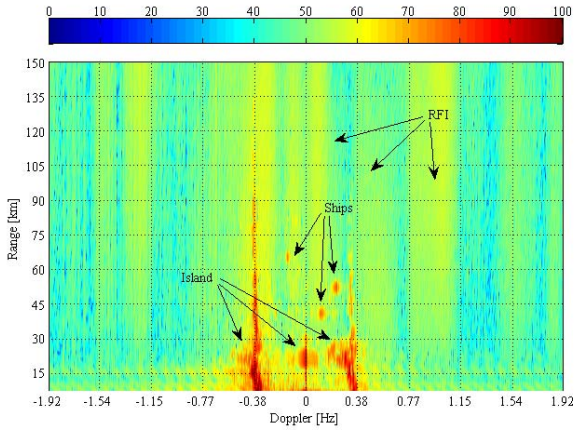

Figure 2. Garchine dataset no. 6: clutter PSD in [dB] for an azimuth angle of 10°.

IV. Auto-Regressive Modeling

A random process $X(n)$ is an auto-regressive (AR) model if it can be described by the following expression:

$$X(n)=\sum_{k=1}^{P} a_{P,k} X(n-k)+W(n), \tag{2}$$

where $a_{P,k}$ (for $k=1,2,...,P$) are the model parameters and $W(n)$ is a white Gaussian process with zero mean and variance σ_W^2. The PSD $S_X^{AR}(f)$ of the process is given by:

$$S_X^{AR}(f)=\frac{\sigma_W^2}{\left|1-\sum_{k=1}^{P} a_k \exp\{-j2\pi kfT\}\right|^2}, \text{ for } |f|<1/2T. \tag{3}$$

Chosen a desired order *P*, the coefficients $a_{P,k}$ are estimated by solving the system of Yule-Walker set of equations expressed by [15], [16]:

$$\hat{\mathbf{a}}_P=\mathbf{R}_X^{-1}\mathbf{r}_X, \tag{4}$$

where:

$$\hat{\mathbf{a}}_P=\left[\hat{a}_{P,1} \quad \hat{a}_{P,2} \quad \cdots \quad \hat{a}_{P,P}\right]^T, \tag{5}$$

$$\mathbf{r}_X=\left[r_X(1) \quad r_X(2) \quad \cdots \quad r_X(P)\right]^T, \tag{6}$$

$$\mathbf{R}_X=\begin{bmatrix} r_X(0) & r_X(1) & \cdots & r_X(P-2) \\ r_X(1) & r_X(0) & \cdots & r_X(P-1) \\ \vdots & \vdots & \ddots & \vdots \\ r_X(P-1) & r_X(P-2) & \cdots & r_X(0) \end{bmatrix}, \tag{7}$$

depend on $r_X(m)$ evaluated from the set of data:

$$r_X(m)\triangleq E\{X(n-m)X^*(n)\}. \tag{8}$$

Then, the estimated variance of the driving process noise is obtained as follows:

$$\hat{\sigma}_W^2=r_X(0)-\sum_{k=1}^{P}\hat{a}_{P,k}r_X(k). \tag{9}$$

Finally, we substitute $\hat{\mathbf{a}}_P$ and $\hat{\sigma}_W^2$, obtained respectively with (4) and (9), in (3).

A. *Modelling accuracy*

Let us consider dataset no. 8 recorded at Brezellec. Some preliminary results are shown in figures 3 and 4, respectively for range cells 21 and 87 and for a common azimuth angle of 0°. They show the comparison between the estimated periodogram (blue line) and the PSD obtained by four AR models: AR(6), AR(12), AR(24) and AR(48), represented by the yellow, green, magenta and red curves respectively.

The main result is that for near range cells, for which the CNR is considerable, second-order peaks can be optimally described only by higher-order models, such as the AR(48) which shows to be the most effective in terms of modeling accuracy of second-order scattering returns (Fig. 3). Low-order AR models are able to follow only the main features of the signal, but not second-order contributes.

Anyway, for distant range cells, second-order Bragg scattering becomes more negligible, thus allowing us to adopt a simpler AR(12) model, which guarantees a good compromise between accuracy and simplicity (Fig. 4). Conversely, low-order AR models tend to generate broad-band first-order Bragg contributes, as done by the AR(6), and even in this case are not suited at all.

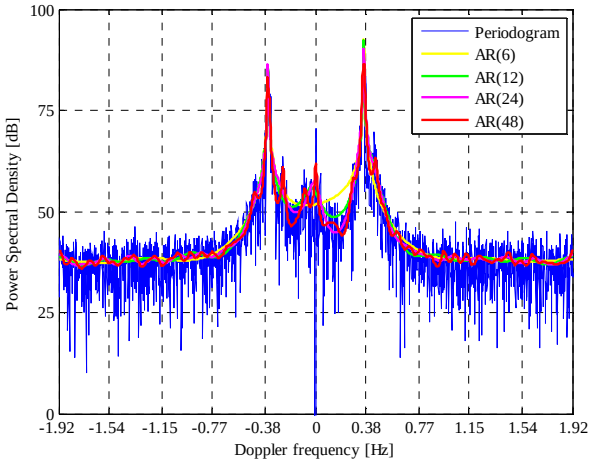

Figure 3. Brezellec dataset no. 8: clutter PSD vs AR modelling in [dB] for range cell 21 and azimuth 0°.

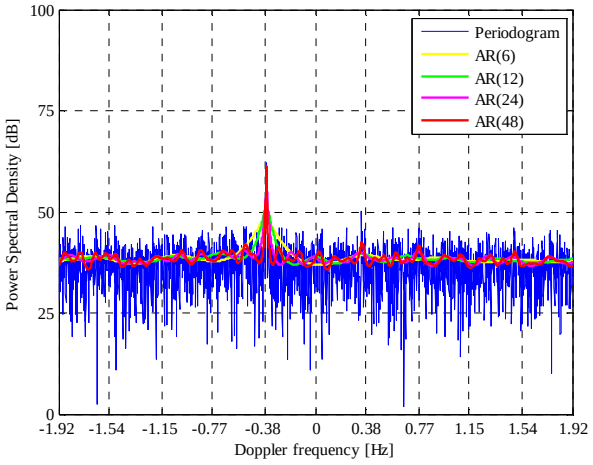

Figure 4. Brezellec dataset no. 8: clutter PSD vs AR modelling in [dB] for range cell 87 and azimuth 0°.

B. Choice of the order P

A common procedure for estimating the most suitable order consists in evaluating the root mean square error (RMSE) of the estimated PSD:

$$RMSE(p) \triangleq \sqrt{\int_{-1/2}^{1/2} \left[S_X(f) - S_X^{AR}(f) \right]^2 df}\,, \qquad (10)$$

where $S_X(f)$ is the empirical PSD of the process estimated from the data (the periodogram) and $S_X^{AR}(f)$ is the AR power spectral density, for a given set of orders (i.e. $p = 2,4,6,\ldots,48$). The choice of $\hat{P}$, for a given RA cell, is done considering the value of p which minimizes the RMSE. The decision-test is given by:

$$\hat{P} : RMSE\left(\hat{P}\right) \equiv \min_p \left\{ RMSE(p) \right\}. \qquad (11)$$

This procedure is carried out for all the cells in RA space (i.e. $N_{RC} = 100$ and $N_{AZ} = 121$, where N_{AZ} is the numer of azimuth cells by which we divided the angle of view after beamforming). The behaviour of $\hat{P}$, based on the test in (11), is plotted against all RA cells, as shown in Fig. 5. The estimated order is generally smaller than 10. However, in some areas $\hat{P}$ is high, as in the high-rigth side of the figure 5 between 40° and 60°. Here clutter is characterized by several peaks in the Doppler frequencies spectrum, thus meaning that the optimal AR order is reasonably high.

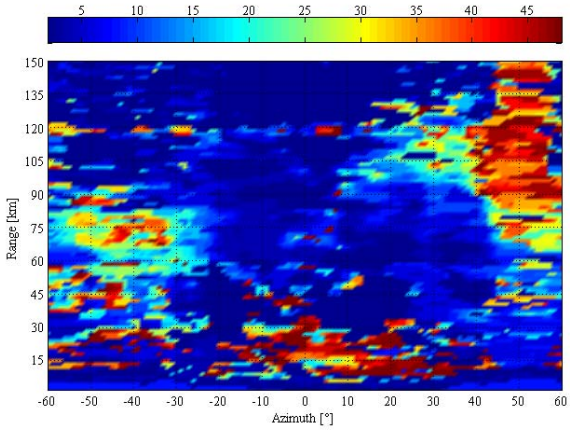

Figure 5. Brezellec dataset no. 8: estimated *P* order at the varying of RA cells.

A further analysis is carried out after averaging the RA profile of $\hat{P}$ over azimuth cells, as shown in Fig. 6. The best choice lies between 10 and 15 for the majority of the cells thus confirming the hypothesis that the AR(12) model is a reasonable good choice. Conversely, higher-order models should be used for modeling near RCs, while lower-order models for distant cells. The peak around RC 80 (about 120 km away from WERA) is caused by the presence of a strong echo near zero Doppler frequencies, as shown in Fig. 1. This peak appears for the majority of azimuth cells.

Concluding, we can state that the AR(12) is a good model both in terms of simplicity and accuracy. Figures 7 and 8 respectively show the range-Doppler (RD) behavior in [dB] of the periodogram and the PSD estimated by means of the AR(12) model, for an azimuth angle of 0°. As we can observe, the main features of the signals are almost always preserved.

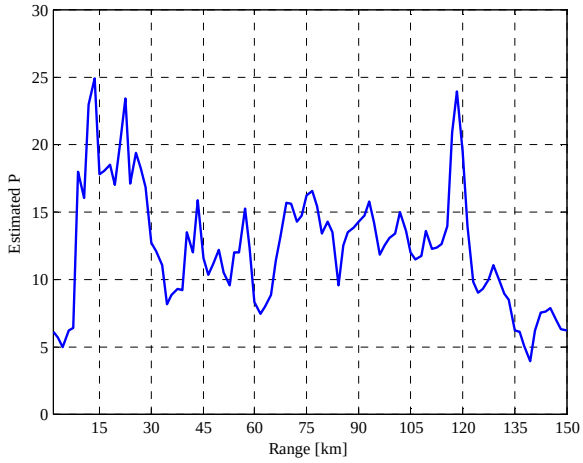

Figure 6. Brezellec dataset no. 8: estimated *P* order as a function of range [km], data have beeen averaged over azimuth.

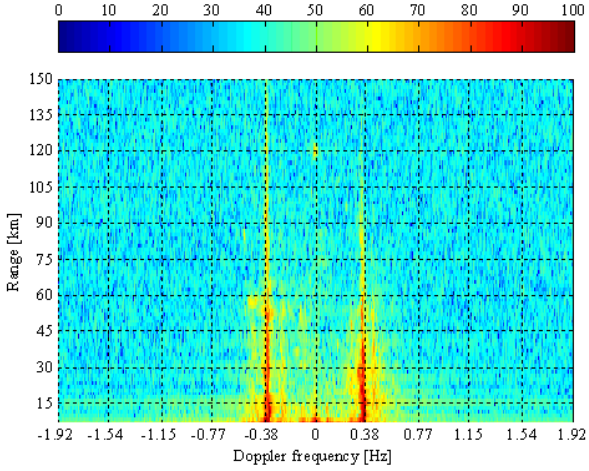

Figure 7. Brezellec dataset no. 8: empiric PSD in [dB] for an azimuth angle of 0°.

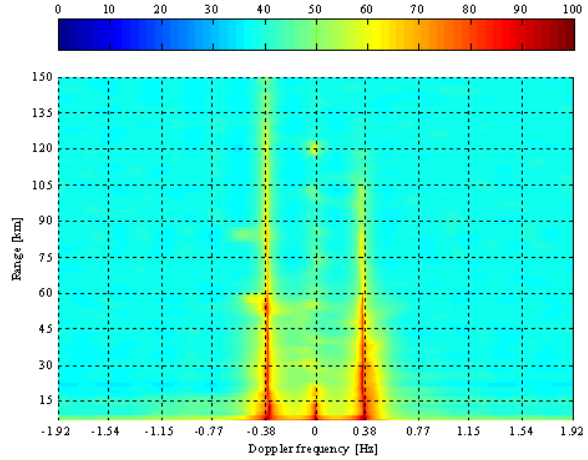

Figure 8. Brezellec dataset no. 8: PSD in [dB] modelled by an AR(12) for an azimuth angle of 0°.

C. Analysis of the poles

In this Section, the poles of the AR model are analyzed and their distribution in the complex plane is discussed [9]. Two cases are presented, both referring to dataset no. 8 recorded at Brezellec: the AR(6) and the AR(10), as shown in figures 9 and 10, respectively. In both cases the poles of the AR models (depicted by blue "x") are considered for all the RCs between 5 and 100. For completeness the two phases corresponding to the advancing and receding Bragg waves are reported as well (red dashed lines).

As expected all the poles are inside the unit circle, thus confirming the stability of the model. Two main accumulation clouds appear very close to the unit circle [9]. This means that the HF signal has two principal narrow-band components.

Usually this pair of poles starts moving from the unit circle towards the centre, where the other poles accumulate. This phenomenon is justified by the fact that with increasing distance, the contribution of sea back-scattering becomes more negligible, as shown in figures 1 and 2. Therefore, the overall signal tends to become a white noise process, as confirmed also by the estimate of the AR order described in Fig. 6, for which the order is generally smaller than 5.

The remaining poles spread inside the unit circle with the same phase spacing and the same radius, except for spurious contributes due to interference sources. The task of these poles consists in describing the "floor" part of the spectrum. With increasing order, they move towards the circle, because the new spectral contributes become even more negligible if compared to the two Bragg components (Fig. 10). In addition, when the order is sufficiently high, the almost-dc component of the signal is described by a pole on the real axis, usually close to the unit circle, especially for near range cells. Concluding, in the case of interferences, new poles are moved towards the disc, for granting and overall good spectral approximation.

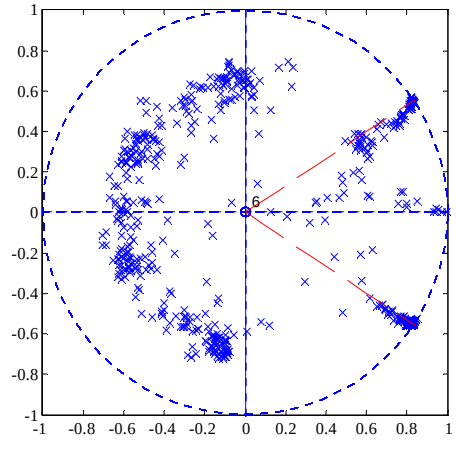

Figure 9. Brezellec dataset no. 8: zeros and poles of the AR(6) model, range cells 5–100 and for an azimuth angle of 0°.

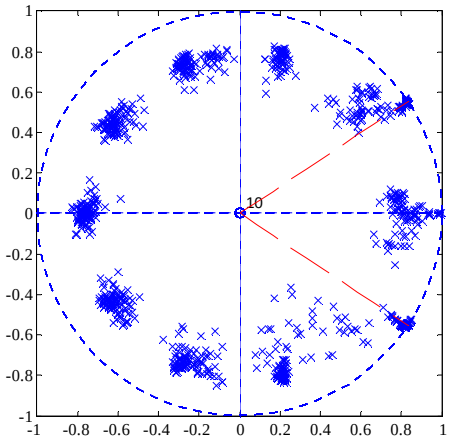

Figure 10. Brezellec dataset no. 8: zeros and poles of the AR(10) model, range cells 5–100 and for an azimuth angle of 0°.

V. CONCLUSIONS

In this paper an accurate analysis of the spectral features of sea clutter in the HF band has been carried out. Initially we provided a qualitative investigation of the main spectral components. Several interesting features were observed. The two Bragg lines which characterize the long-term sea clutter variations are well defined for the majority of cells. On the contrary, the second order peaks, which are instead responsible of the rapid changes in the wave behavior, are well defined only for near range cells. The contribution of land scattering can be observed as well (but only for near mixed sea/land cells) in addition with unwanted signals, both man-made and natural. Variations in the RD profile strongly depend on the angle of view, after beamforming. In the second part we presented a common AR modeling technique. Our results have evidenced that only for low CNR levels it is possible to describe the clutter signal with a reasonably low-order AR model. For reducing the spectral parameters under estimations, we tried also a different parametric model composed of simple functions as the Gaussian and the exponential. Unfortunately, the results were not promising and we decided to omit them. The ARMA modelling is currently under investigation and will be presented in future works.

ACKNOWLEDGMENT

The authors would like to express their sincere gratitude to Riccardo Tinti for his precious help.

REFERENCES

[1] J. M. Headrick, and M. I. Skolnik, “Over-the-Horizon Radar in the HF Band,” Proceedings of the IEEE, vol. 62, no. 6, pp. 664-673, June 1974.

[2] K. W. Gurgel, H. H. Essen, and S. P. Kingsley, “High-frequency radars: physical limitations and recent developments,” Coastal Engineering, vol. 37, no. 3, pp. 201-218, August 1999.

[3] K. W. Gurgel, G. Antonischki, H. H. Essen, and T. Schlick, “Wellen Radar (WERA): a new ground-wave radar for ocean remote sensing,” Coastal Engineering, vol. 37, no. 3, pp. 219-234, August 1999.

[4] A. M. Ponsford, L. Sevgi, and H. C. Chan, "An Integrated Maritime Surveillance System Based on High-Frequency Surface Wave radars. Part 2: Operational Status and System Performance," IEEE Antennas and Propagation Magazine, vol. 43, no. 5, pp. 52-63, October 2001.

[5] A. M. Ponsford, "Surveillance of the 200 Nautical Mile Exclusive Economic Zone (EEZ) Using High Frequency Surface Wave Radar (HFSWR)," Canadian Journal on Remote Sensing, vol. 27, no. 4, Special Issue on Ship Detection in Coastal Waters, pp. 354-360, August 2001.

[6] D. D. Crombie, “Doppler Spectrum of Sea Echo at 13.56 Mc/s,” Nature 175, pp. 681-682, 1955.

[7] D. E. Barrick, “First-Order Theory and Analysis of MF/HF/VHF Scatter from the Sea,” IEEE Transactions on Antennas and Propagation, vol. 20, no.1, pp. 2-10, January 1972.

[8] G. A. Fabrizio, “Space-Time Characterisation and Adaptive Processing of Ionospherically-Propagated HF Signals,” Doctoral Philosophy Thesis Dissertation, July 2000.

[9] R. H. Khan, “Ocean-Clutter Model for High-Frequncy Radar,” IEE Journal of Oceanic Engineering, vol. 16, no. 2, pp. 181-188, April 1991.

[10] R. J. Martin, and M. J. Kearney, “Remote Sea Current Sensing Using HF Radar: An Autoregressive Approach,” IEEE Journal of Oceanic Engineering, vol. 22, no. 1, pp. 151-155, January 1997.

[11] S. Maresca, M. Greco, F. Gini, R. Grasso, S. Coraluppi, and N. Thomas, “The HF Surface Wave Radar WERA. Part I: Statistical Anlaysis of Recorded Data, *IEEE Radar Conference 2010*, Washington DC, USA, May 2010.

[12] K. W. Gurgel, Y. Barbin, and T. Schlick, “Radio Frequency Interference Suppression Techniques in FMCW Modulated HF Radars,” Proceedings of Oceans 2007 Europe, Aberdeen (Scotland), pp. 4, June 2007.

[13] http://ifmaxp1.ifm.zmaw.de/WERA.shtml

[14] M. Greco, S. Maresca, F. Gini, R. Grasso, and S. Coraluppi, “Statistical Analysis Measured by the HF Surface Wave Radar WERA,” *NATO Workshop on Data Fusion and Anomaly Detection for Maritime Situation Awareness*, La Spezia, Italy, Septmeber 2009.

[15] S. M. Kay, and L. Marple, “Spectrum Analysis - A modern perspective,” Proceedings of the IEEE, vol. 69, no. 11, pp. 1380-1419, November 1981.

[16] P. Stoica, and R. Moses, “Spectral Analysis of signals,” Pearson Prentice Hall, 2005